Available online at www.sciencedirect.com

ScienceDirect

Procedia Structural Integrity 38 (2022) 141–148

Structural Integrity Procedia

www.elsevier.com/locate/procedia

FATIGUE DESIGN 2021, 9th Edition of the International Conference on Fatigue Design

Contribution of the introduction of artificial defects by additive manufacturing to the determination of the Kitagawa diagram of Al-Si alloys

M. Bonneric[a,*], C. Brugger[a], N. Saintier[a], A. Castro Moreno[b], B. Tranchand[b]

[a]*Arts et Métiers Institute of Technology, University of Bordeaux, CNRS, Bordeaux INP, INRAE, HESAM Université, I2M, Esplanade des Arts et Métiers, 33400 Talence, FRANCE*

[b]*IRT Saint-Exupery, 3 rue Tarfaya, 31400 Toulouse, FRANCE*

Abstract

Despite the continuous progress in the additive manufacturing (AM) technologies to improve the quality of the produced parts, the presence of defects induced by the process remains a critical issue for the design of industrial components with respect to fatigue damage. Analytical models such as Kitagawa diagrams represent easy to use tools to predict fatigue strength accounting for the detrimental influence of the defects. They are therefore of great interest from an industrial point of view. The aim of the present work is to evaluate whether artificial defects obtained by placing holes directly into the CAD files of fatigue specimens can be used to establish Kitagawa diagrams, despite some differences in terms of shapes and morphologies between the natural and artificial defects. Two artificial defect geometries with a similar size were studied. For each of these geometries, the experimental fatigue strengths and the real sizes of the critical defects measured from the fracture surfaces were used to determine the parameters of the El-Haddad model. For one of the geometries, the obtained model was able to predict the fatigue strength corresponding to the natural defects, and the associated parameters were found consistent with the literature. The fatigue tests results also highlighted the influence of the defect shape.

* Corresponding author.
E-mail address: matthieu.bonneric@ensam.eu

2452-3216
10.1016/j.prostr.2022.03.015

Keywords: Fatigue ; Additive manufacturing ; Al-Si alloy ; Artificial defect ;

Nomenclature

$\sigma_{max,D}$	fatigue resistance expressed in terms of maximum stress over a cycle
$\sigma_{max,D0}$	fatigue resistance in the absence of defects used for the El-Haddad model
$\sqrt{area}_0$	El-Haddad parameter expressed in terms of the Murakami parameter
$\Delta K_{th,lc}$	long crack propagation threshold

1. Introduction

The manufacturing of parts by laser powder bed fusion (L-PBF) technology usually involves the generation of defects such as gas pores or lack-of-fusion defects [1], [2]. It is now well established that these defects are one of the main causes of fatigue damage in additively manufactured (AM) parts [3], [4], the other one being the surface roughness [5]. Predicting the fatigue strength from defects is therefore of great interest to improve the reliability of AM parts, in particular for Al-Si alloys for which defects might not be fully eliminated, even with post-treatments such as Hot Isostatic Pressing (HIP) [6], [7].

The presence of defects being a common issue for conventional processes, substantial literature exists on the sensitivity of the fatigue behavior to defects. Murakami's works on the subject [8] showed that the main defect characteristics that impact on the fatigue strength are the *defect size*, *defect position* (surface, sub-surface or internal), *defect shape* (spherical, tortuous, etc…), and *defect type* (pore, inclusion, etc…). Among these features, the position with respect to the surface and the size appear to be the key parameters since a) critical fatigue cracks usually initiate at surface or sub-surface defects in the HCF regime b) in many cases the fatigue strength can be properly assessed using the Kitagawa-Takahashi diagram [9]–[11], which describes the evolution of the fatigue resistance as a function of the size of the defect responsible for fatigue failure. In particular, it should be noted that a correct prediction of the Kitagawa diagram can be obtained for AM Al-Si alloys [5], [12].

To obtain relevant experimental data to parameterize models of the Kitagawa diagram, artificial defects of controlled sizes and shapes can be introduced on the surface of fatigue specimens, for example by micro-drilling [13], or by EDM [14]. The use of artificial defects not only tends to limit the scattering of the fatigue test results, the defect sizes and shapes being controlled, but also enables the investigation of a wide range of defect sizes. In this context, the present work aims to evaluate whether artificial defects obtained by placing holes directly into the CAD files of fatigue specimens [15], [16] can be used to establish the Kitagawa diagram of the AM AlSi7Mg0.6 alloy, despite the differences in terms of morphologies between the natural and artificial defects. To do so, two artificial defect geometries were considered, corresponding to a same defect size but two distinct morphologies. Surface defects were introduced into fatigue specimens which were subjected to fatigue tests at a load ratio of R=0.1. The fatigue resistance was assessed using the staircase method for each defect type, and the critical defects sizes were measured from SEM observations. These data were used to determine the parameters of the El-Haddad model [17] for each defect type. The results were discussed by comparing the predictions of the obtained models with fatigue test results associated to natural defects.

2. Materials and Methods

2.1. Material

Samples with artificial defects (see section 2.2) were produced on a SLM 280HL powder bed machine on the additive manufacturing platform (FUTURPROD) of I2M institute, using the AlSi7Mg0.6 aluminium alloy. The process parameters recommended by the manufacturer for Al-Si alloys were used (see Table 1), and the powders

were dried under inert environment at 150°C for 12 h prior to the manufacturing. All samples were built in the vertical direction. They were then subjected to a T6 heat-treatment, consisting in a solution treatment at 535°C for 2 h, followed by a water quenching and an artificial aging at 170 °C for 4 h. Observations of the resulting microstructures can be found in **[7]**, as well as the analysis of the natural defect population associated to the process parameters used for the manufacturing. Fatigue specimens, whose dimensions are provided in Figure 1, were machined after heat-treatment in order to prevent from the influence of the surface roughness on the fatigue behavior, and then promote fatigue crack initiation at the artificial defects.

Table 1. Process parameters recommended for Al-Si alloys.

Layer thickness	Laser power	Scan velocity	Hatch spacing	Scanning strategy	Base plate heating	Atmosphere
30µm	350W	1650mm/s	130µm	Stripes	150°C	Argon

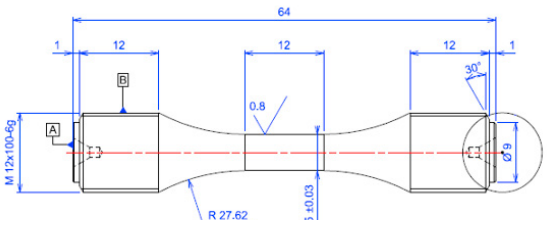

Figure 1: Geometry of the machined specimens used for the HCF fatigue tests

2.2. Artificial defects

Artificial defects were generated in the samples by introducing holes directly into the CAD files of the manufactured samples. Two batches of fatigue specimens were considered, each one corresponding to a defect geometry. In a previous work, subsurface defects had already been obtained by this method, considering either spherical holes of diameter 450µm or ellipse-shaped holes of diameter 600µm and height 300µm [15]. It was found that the fatigue strength at 2×10^6 cycles is greatly sensitive to the thickness of the bridge of matter between the

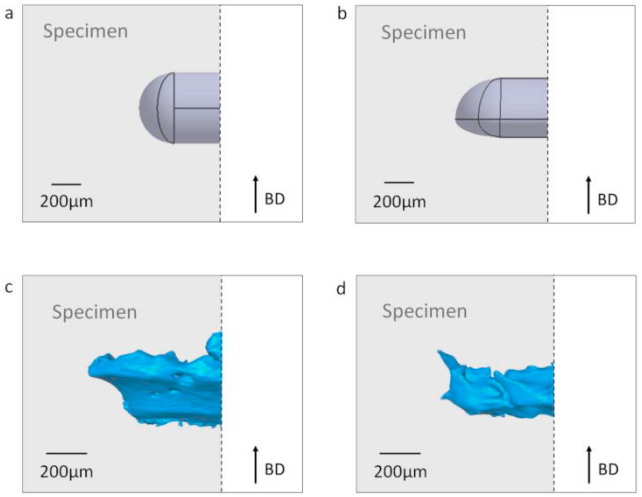

Figure 2: Comparison of the resulting artificial defects observed with X-ray tomography with the corresponding CAD geometries (BD = Building Direction). a) CAD geometry for defect #1. b) CAD geometry for defect #2. c) Actual defect #1 d) Actual defect #2.

defect and the specimen surface. As it is difficult to accurately control this parameter due to the uncertainty associated to machining stage, surface defects were considered in this study instead of subsurface ones, with the aim of reducing the scattering of the fatigue test data. To do so, the hole geometries described above were modified to connect the hole to the surface, as illustrated in Figures 2a and 2b. For example, the modified geometry for the spherical holes is a cylinder of diameter 450µm ending in a hemisphere of the same diameter. In what follows, the defects resulting from the spherical geometry and the ellipse-shaped hole geometry will be designated as defects #1 and defects #2, respectively. Figures 2c and 2d provide CT scan views of the actual defects obtained when introducing such holes. One can see that the defect shapes are not entirely controlled and differ from the CAD. This was also observed in previous work involving subsurface defects, where the defects had been obtained with a satisfying reproducibility in terms of $\sqrt{area}$ with a standard deviation of less than 10%. For each geometry, the depth of the hole was chosen so that after the machining stage the defect size $\sqrt{area}$ is approximately 600µm, corresponding to larger defect sizes compared to natural defects [7] to promote the critical fatigue crack initiation at the artificial defects.

2.3. Fatigue testing conditions

Tension/tension fatigue tests were conducted on a Zwick resonant machine at room temperature in air and at a frequency of 80 Hz. All specimens were tested applying a R = 0.1 load ratio. The stop criterion was a frequency drop of 0.5 Hz corresponding to a crack of approximately 1.5 mm in depth, or a maximum number of cycles of 2×10^6 cycles. The staircase method was used to assess the fatigue resistance at 2×10^6 cycles. Following this procedure, each specimen was tested at one stress level only. The step between two levels was 5MPa. The non-broken specimens were also subjected to a Locati procedure by steps of 5MPa until failure was detected, in order to measure the sizes of the critical defect through SEM observations. However the results from these Locati procedures were not reported in the S-N curve presented hereafter.

3. Results and Discussion

3.1. Fatigue testing results

Figure 3 shows the S-N curves associated to the staircase procedures applied to the two batches of specimens considered in this study. The evaluated fatigue resistances at 2×10^6 cycles were $\sigma_{max,D} = 69MPa \pm 5MPa$ and $\sigma_{max,D} = 85MPa \pm 5MPa$ for defect #1 specimens and defect #2 specimens, respectively. SEM observations of the fracture surfaces confirmed that the critical fatigue cracks initiated at the artificial defects (see Figure 4), and the sizes of the defects #1 and defects #2 were found to be $625\mu m \pm 70\mu m$ and $580\mu m \pm 15\mu m$, respectively. As

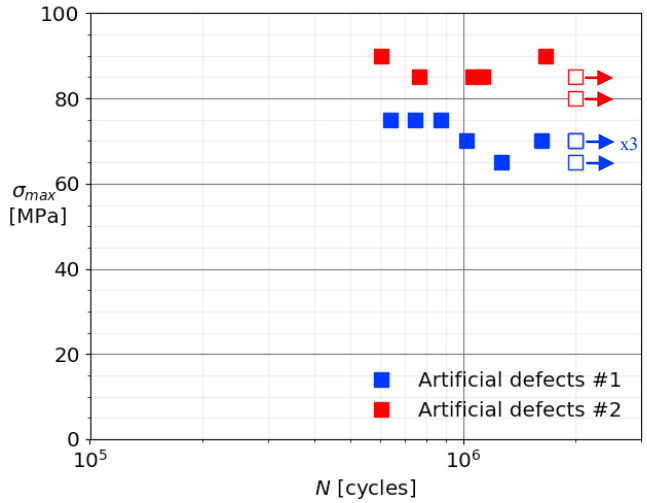

Figure 3: S-N curves associated to the staircase method used to test the specimens

expected, the initiation of fatigue cracks at artificial defects of controlled sizes, position and shapes lead to a limited scattering of the results. In addition, a significant decrease of the fatigue resistance was observed when comparing the results with those associated to specimens produced in the same conditions but without any artificial defects [7], for which the fatigue resistance at 2×10^6 cycles was found to be $\sigma_{max,D} = 152MPa \pm 8MPa$. This decrease can be attributed to the size of the artificial defects which is much larger than the sizes of the natural critical defects involved in [7] that were ranging from 20µm to 120µm.

The present results also suggest a non-negligible influence of the artificial defect morphology on the fatigue strength, as the fatigue resistance associated to defects #2 is 23% higher than for defects #1 despite similar defect sizes.

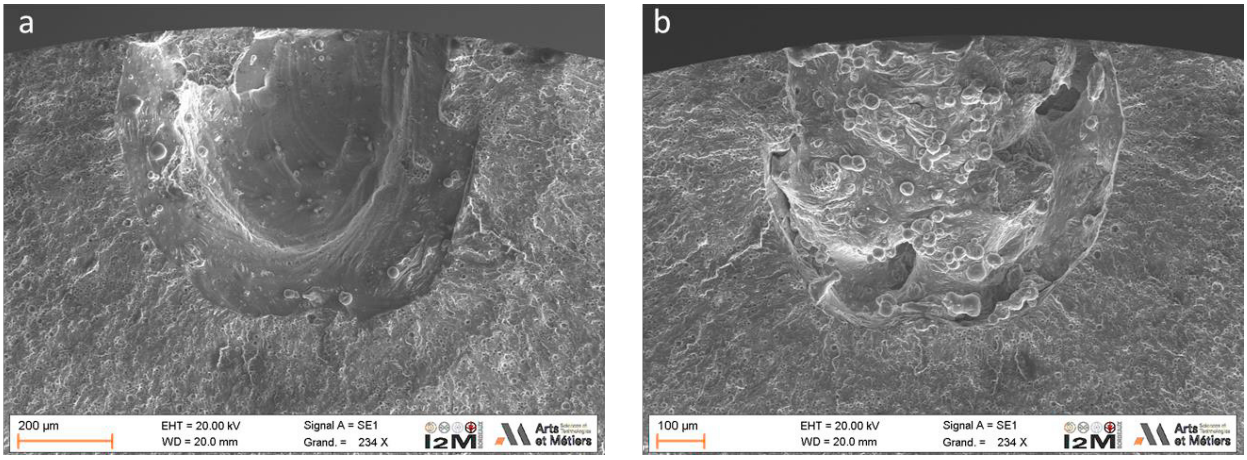

Figure 4: SEM observations of the fracture surfaces associated to a critical defect #1 of size $\sqrt{area} = 640\mu m$. a) Lower part of the defect with respect to the building direction. b) Upper part of the defect with respect to the building direction.

3.2. Kitagawa diagram

The fatigue strength at 2×10^6 cycles in presence of defects can be evaluated using the Kitagawa-Takahashi diagram, which describe the evolution of the fatigue resistance as a function of the critical defect size [9]. Among the many formulations to model this diagram, El-Haddad's one [17] is very simple and allows to predict the fatigue strength using Eq. 1 below :

$$\sigma_{max,D} = \sigma_{max,D0} \sqrt{\frac{\sqrt{area}_0}{\sqrt{area} + \sqrt{area}_0}} \qquad (1)$$

where $\sigma_{max,D0}$ is the fatigue strength in the absence of defect and $\sqrt{area}_0$ the El-Haddad's parameter expressed in terms of the Murakami $\sqrt{area}$ parameter. The fatigue strength in the absence of defect was estimated as the stress value corresponding to a plastic deformation of 0.05% on the stabilized cyclic stress-strain curve, as in [12]. The latter one was obtained by conducting strain-imposed tension cyclic tests. Standard machined specimens were tested on a MTS servo-hydraulic testing machine at a strain amplitude $\varepsilon = \pm 0.5\%$ with a frequency f=0.1Hz. The parameter $\sigma_{max,D0}$ was therefore assessed to 200MPa. The parameter $\sqrt{area}_0$was determined using the fatigue test results associated to the artificial defects. To do so, the long crack threshold $\Delta K_{th,lc}$ was determined for each defect type using Eq. 2 [18] to be used in Eq. 3 to compute $\sqrt{area}_0$.

$$\Delta K_{th,lc} = 0.65\,\Delta\sigma_D\sqrt{\pi\sqrt{area}} \quad (2)$$

$$\sqrt{\text{area}}_0 = \frac{1}{\pi}\left(\frac{\Delta K_{th,lc}}{0.65\Delta\sigma_D}\right)^2 \quad (3)$$

The El-Haddad parameter was evaluated to $\sqrt{\text{area}}_0 = 75\mu m$ using the results for artificial defects #1, and $\sqrt{\text{area}}_0 = 105\mu m$ using the results for artificial defects #2. One should note that the value found for defects #1 also corresponds to the El-Haddad parameter determined in [12] for the as-built AlSi10Mg. Figure 5 shows the predictions of the Kitagawa diagram using the obtained parameters for the El-Haddad model. The experimental fatigue strengths at 2×10^6 cycles plotted as a function of the mean defect size measured on the fracture surfaces are also indicated for the natural defects [7], defects #1 and defects #2. As the data associated to the natural defects were not used to parameterize the models, one may consider the model responses for the mean natural defect size for validation. Both models provide a correct assessment of the fatigue resistance associated to the natural defects, although the model associated to defects #1 is more satisfying as it provides a conservative evaluation. The results therefore suggest that the artificial defects considered in this study can be used to establish the Kitagawa diagram despite their differences in terms of shapes compared to the natural defects.

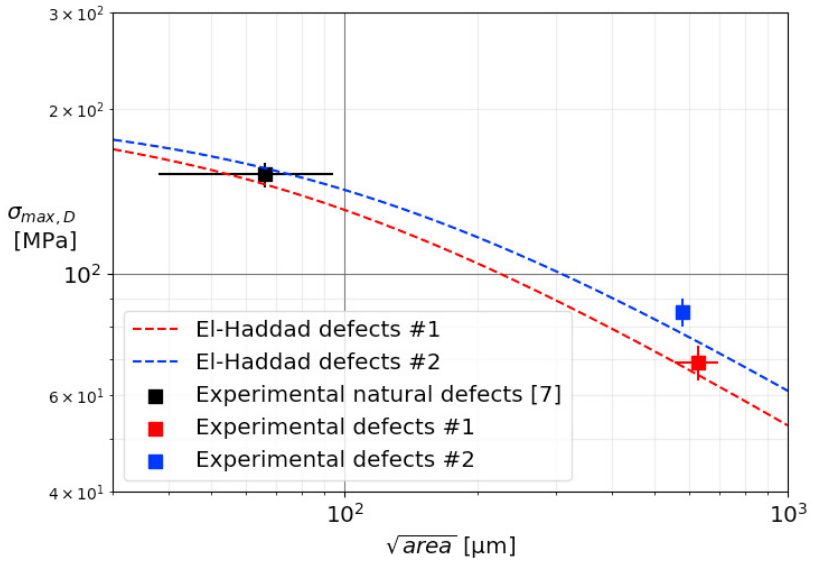

Figure 5: Kitagawa diagram for the fatigue resistance at 2.10^6 cycles for load ratio of R=0.1

4. Conclusions

In this work, it was proposed to introduce artificial defects directly into the CAD files of additively manufactured specimens to establish the Kitagawa Takahashi diagram of the AlSi7Mg0.6 alloy. The fatigue cracks successfully initiated at the artificial defects, resulting in a limited scatter of the results. In addition, the El-Haddad model determined with artificial defect data provided a satisfying prediction of the fatigue strength associated to the natural defects. At the present time, further numerical work is being carried out to study the influence of the artificial defect morphology, as some differences in terms of fatigue strengths were observed between the different artificial defect geometries considered in this study.

Acknowledgements

This work falls within the framework of the ANDDURO project hosted by the French Institute of Technology IRT Saint Exupery, supported by Occitanie Region and industrial partners. In addition, the specimens were produced on the FUTURPROD additive manufacturing platform of I2M Institute.

References

[1] E. O. Olakanmi, R. F. Cochrane, et K. W. Dalgarno, « A review on selective laser sintering/melting (SLS/SLM) of aluminium alloy powders: Processing, microstructure, and properties », *Progress in Materials Science*, vol. 74, p. 401-477, 2015, doi: 10.1016/j.pmatsci.2015.03.002.

[2] B. Zhang, Y. Li, et Q. Bai, « Defect Formation Mechanisms in Selective Laser Melting: A Review », *Chinese Journal of Mechanical Engineering*, vol. 30, n° 3, p. 515-527, 2017, doi: 10.1007/s10033-017-0121-5.

[3] N. Sanaei, « Defects in additive manufactured metals and their effect on fatigue performance: A state-of-the-art review », *Progress in Materials Science*, p. 41, 2021.

[4] S. Siddique, M. Imran, E. Wycisk, C. Emmelmann, et F. Walther, « Influence of process-induced microstructure and imperfections on mechanical properties of AlSi12 processed by selective laser melting », *Journal of Materials Processing Technology*, vol. 221, p. 205-213, 2015, doi: 10.1016/j.jmatprotec.2015.02.023.

[5] S. Beretta, M. Gargourimotlagh, S. Foletti, A. du Plessis, et M. Riccio, « Fatigue strength assessment of "as built" AlSi10Mg manufactured by SLM with different build orientations », *International Journal of Fatigue*, vol. 139, 2020, doi: 10.1016/j.ijfatigue.2020.105737.

[6] W. H. Kan, Y. Nadot, M. Foley, L. Ridosz, G. Proust, et J. M. Cairney, « Factors that affect the properties of additively-manufactured AlSi10Mg: Porosity versus microstructure », *Additive Manufacturing*, vol. 29, p. 100805, 2019, doi: 10.1016/j.addma.2019.100805.

[7] M. Bonneric, C. Brugger, et N. Saintier, « Effect of hot isostatic pressing on the critical defect size distribution in AlSi7Mg0.6 alloy obtained by selective laser melting », *International Journal of Fatigue*, vol. 140, 2020, doi: 10.1016/j.ijfatigue.2020.105797.

[8] Y. Murakami, *Metal Fatigue: Effects of Small Defects and Nonmetallic Inclusions*, Elsevier. 2002.

[9] T. S. Kitagawa, « Applicability of fracture mechanics to very small cracks », *ASM Proceedings of 2nd international conference on mechanical Metalspark*, p. 627-631, 1976.

[10] M. Vincent, Y. Nadot, C. Nadot-Martin, et A. Dragon, « Interaction between a surface defect and grain size under high cycle fatigue loading: Experimental approach for Armco iron », *International Journal of Fatigue*, vol. 87, p. 81-90, 2016, doi: 10.1016/j.ijfatigue.2016.01.013.

[11] V.-D. Le, F. Morel, D. Bellett, N. Saintier, et P. Osmond, « Simulation of the Kitagawa-Takahashi diagram using a probabilistic approach for cast Al-Si alloys under different multiaxial loads », *International Journal of Fatigue*, vol. 93, p. 109-121, 2016, doi: 10.1016/j.ijfatigue.2016.08.014.

[12] S. Romano, A. Brückner-Foit, A. Brandão, J. Gumpinger, T. Ghidini, et S. Beretta, « Fatigue properties of AlSi10Mg obtained by additive manufacturing: Defect-based modelling and prediction of fatigue strength », *Engineering Fracture Mechanics*, vol. 187, p. 165-189, 2018, doi: 10.1016/j.engfracmech.2017.11.002.

[13] E. Pessard, M. Lavialle, P. Laheurte, P. Didier, et M. Brochu, « High-cycle fatigue behavior of a laser powder bed fusion additive manufactured Ti-6Al-4V titanium: Effect of pores and tested volume size », *International Journal of Fatigue*, vol. 149, 2021, doi: 10.1016/j.ijfatigue.2021.106206.

[14] J. N. Domfang Ngnekou *et al.*, « Fatigue properties of AlSi10Mg produced by Additive Layer Manufacturing », *International Journal of Fatigue*, vol. 119, p. 160-172, 2019, doi: 10.1016/j.ijfatigue.2018.09.029.

[15] M. Bonneric, C. Brugger, et N. Saintier, « Investigation of the sensitivity of the fatigue resistance to defect position in aluminium alloys obtained by Selective laser melting using artificial defects », *International Journal of Fatigue*, vol. 134, 2020, doi: 10.1016/j.ijfatigue.2020.105505.

[16] O. Andreau, E. Pessard, I. Koutiri, P. Peyre, et N. Saintier, « Influence of the position and size of various deterministic defects on the high cycle fatigue resistance of a 316L steel manufactured by laser powder bed fusion », *International Journal of Fatigue*, vol. 143, 2021, doi: 10.1016/j.ijfatigue.2020.105930.

[17] M. H. El Haddad, T. H. Topper, et K. N. Smith, « Prediction of non propagating cracks », *Engineering Fracture Mechanics*, vol. 11, n° 3,

p. 573-584, 1979, doi: 10.1016/0013-7944(79)90081-X.
[18] Y. Murakami, « Analysis of stress intensity factors of modes I, II and III for inclined surface cracks of arbitrary shape », *Engineering Fracture Mechanics*, vol. 22, n° 1, p. 101-114, 1985, doi: 10.1016/0013-7944(85)90163-8.